An Analytical-Numerical Model for Two-Phase Slug Flow through a Sudden Area Change in Microchannels

A. Mehdizadeh Momen[1], S.A. Sherif[2†] and W. E. Lear[2]

[1] *Building Technologies Research and Integration Center Oak Ridge National Laboratory Oak Ridge, TN, USA*

[2] *Department of Mechanical and Aerospace Engineering, University of Florida, P.O, Box 116300, USA*

†*Corresponding Author Email: Sasherif@ufl.edu*

ABSTRACT

In this paper, two new analytical models have been developed to calculate two-phase slug flow pressure drop in microchannels through a sudden contraction. Even though many studies have been reported on two-phase flow in microchannels, considerable discrepancies still exist, mainly due to the difficulties in experimental setup and measurements. Numerical simulations were performed to support the new analytical models and to explore in more detail the physics of the flow in microchannels with a sudden contraction. Both analytical and numerical results were compared to the available experimental data and other empirical correlations. Results show that models, which were developed based on the slug and semi-slug assumptions, agree well with experiments in microchannels. Moreover, in contrast to the previous empirical correlations which were tuned for a specific geometry, the new analytical models are capable of taking geometrical parameters as well as flow conditions into account.

NOMENCLATURE

A	pipe cross sectional area	X_c	liquid slug center of mass f friction factor
D	pipe diameter		
f_f	wall shear stress		
G	total mass flux	β	homogenous gas void fraction
J_g	gas phase superficial velocity	ε	roughness
J_l	liquid phase superficial velocity	u_f	front slug velocity
$\dot{m}_t$	total mass flow rate	μ_g	gas phase viscosity
$\dot{m}_l$	liquid slug mass	u_g	gas slug velocity
$\dot{m}_g$	gas slug mass	α	gas volume void fraction
K_c	contraction loss coefficient	μ_l	liquid phase viscosity
K_d	momentum correction factor	u_l	liquid slug velocity
K_e	expansion loss coefficient	σ	slip ratio
X	vapor mass quality		

1. INTRODUCTION

The study of flow in microchannels has become of greater interest in recent years mainly due to its presence in a broad array of applications such as microelectromechanical systems (MEMS), electronics cooling, chemical process engineering, medical and genetic engineering, and bioengineering.

Two-phase hydrodynamic characteristics in microchannels have been found to be different than those in large channels. Recent experimental studies by Ghiaasiaan and Abdel-Khalik (2000), Abdelall *et al.* (2005), Toufik *et al.* (2008), Kawahara *et al.* (2002), Serizawa *et al.* (2002), Chaoqun *et al.* (2013), Kawahara *et al.* (2012), Yao *et al.* (2014) and many others tried to formulate and monitor flow in

microchannels. However, there are still discrepancies in the data, mainly due to the difficulties in experimental setup and measurement. On the other hand, there are very few analytical or numerical studies in two-phase flows in microchannels mainly due to the lack of the detailed experimental data or robust physical-based models for simulation. He and Kasagi (2008) simulated a single bubble in a micro tube. Fukagata *et al*. (2007) numerically simulated two-phase flow in a micro tube and found that the gas-liquid slip ratio is approximately 1.2. They also found that this was in accordance with the Armand correlation which is valid for two phase flows in micro-sized channels. The presented analytical model in that study also revealed that the calculated void fraction in an abrupt flow area contraction was close to the Armand correlation for many data points, but for some points (depending on the flow conditions) could have up to a twenty percent bigger value, which leads to better agreement with experimental data. De Schepper *et al*. (2008), utilizing CFD simulation, investigated the performance of the existing numerical tools and approaches for modeling of two phase flows. Their qualitative comparisons between computed contours and the experimental photos showed that simulation could capture two-phase flow regimes except for slug flow. They tried all available two-phase models to overcome this problem; however, their simulation failed in capturing the slug flow regime both qualitatively and quantitatively. They attributed this fact to the presence of a small region of slug flow in the Baker chart. A consequence of this is the fact that their simulations were vulnerable to transition between regions.

Two-phase flow in microchannels with abrupt area change is among the least studied aspects of this type of flow. The objective of the work reported in this paper is to provide a new analytical void fraction model in the vicinity of the area transition (*vena contracta* location) for two-phase slug flows and to apply this model to estimate the pressure drop due to the abrupt area change in microchannels. Compared to previous models, which provide a static value for the void fraction without geometrical or flow constraints, the new model provides an analytical expression for the void fraction that accounts for both dynamic and static variables. Also, this model introduces a geometrical parameter that has historically been ignored in previous experimental work. This is the average liquid slug length and/or the gas slug length. The ratio of these two lengths can be calculated by knowing the void fraction, but the actual length of each slug can vary depending on the flow conditions. Since the slug flow through the contraction behaves like pulsating flow, the actual length of each slug (in addition to the gas-liquid slug's length) plays an important role on the calculated pressure drop. Moreover, it is expected that the actual length of the slugs controls whether or not the boundary layer is located in the developing region in each slug. We suggest that future experimental efforts report detailed data about the time-averaged slug lengths of the two phases as well.

2. ANALYSIS

2.1 Two-Phase Slug Flow Frictional Pressure Drop in a Straight Microchannel

Damianides and Westwater (1988), Fukano and Kariyasaki (1993), Triplett *et al*. (1999), Zhao and Bi (2001) and Kawahara *et al*. (2002) developed overall two-phase flow regime maps taking into account a wide range of parameters in microchannels. Kawahara *et al*. (2002) did not observe any bubbly or churn flow patterns in their developed map for a 100-μm microchannel. On the other hand, for a wide range of gas and liquid superficial velocities, the slug-ring, ring-slug, multiple and semi-annular flows were observed.
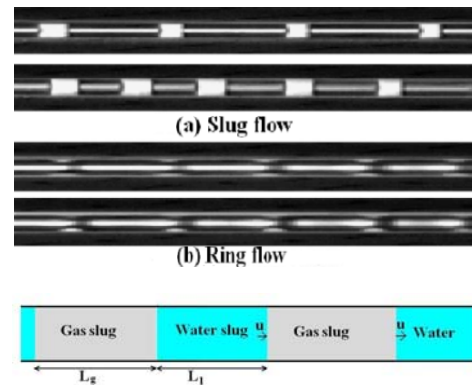

Fig. 1. Top: Experimental image, Serizawa *et al*. (2002). Bottom: Schematic picture of two-phase slug flow in a straight microchannel.

For slug flow it can be assumed that pressure drop is due to the additive pressure drop of separate liquid and gas phases. Here we assume that a gas slug and a liquid slug follow each other, that there is no mass transfer between the phases, that the gas phase is incompressible in the channel (This assumption would not be valid for the abrupt area change region since the pressure changes noticeably in a short distance in that region), and that these slugs have the same velocity (see Fig. 1). This is completely different than homogenous flow in which both phases are so mixed to each other to behave as new homogenous flow in which it is normally assumed that both phases have the same velocity. In other words, it is assumed that the slip ratio is unity for homogeneous flow while the slip ratio definition for slug flow in microchannels when there is periodic dry wall is not clear. The mass flow rate of gas and liquid in a microchannel can be written as

$$\dot{m}_g = \rho_g A J_g \tag{1}$$

$$\dot{m}_l = \rho_l A J_l \tag{2}$$

where J_g and J_l are the superficial velocities of the gas and liquid phases, respectively. A is the cross sectional area of the circular microchannel and ρ_g

and ρ_l are the densities of the gas and liquid phases, respectively. Therefore the total mass flow rate can be expressed as

$$\dot{m}_t = A(\rho_g J_g + \rho_l J_l) \tag{3}$$

As we mentioned, since the mass flux across the gas-liquid interface is zero in the interface frame of reference, the velocity of both phases can be assumed to be the same, $u_g = u_l = u$; therefore the velocity of the slugs in the stationary frame of reference can be written as

$$u = \frac{\rho_g J_v + \rho_l J_l}{\alpha \rho_g + (1-\alpha)\rho_l} = \frac{G}{\alpha \rho_g + (1-\alpha)\rho_l} \tag{4}$$

in which α is the gas phase void fraction that is equal to the homogenous gas void fraction, β, for slug flows in microchannels and G is the total mass flux (kg/s.m^2) of the two-phase flow. In the slug flow, for each phase, we have assumed that the flow is fully developed except close to the interfaces. This assumption may be reasonable only for relatively long slugs. For each phase, assuming a parabolic laminar, fully-developed velocity profile, the pressure gradient would have the same form as for laminar pipe flow, with a time weighting correction.

$$(\frac{\Delta P}{\Delta x})_{2\Phi} = \frac{32\mu_g u_g}{D^2}\alpha + \frac{32\mu_l u_l}{D^2}(1-\alpha) \tag{5}$$

This means that at a certain location of the channel, in α portion of the time in which only the gas phase exists, the pressure gradient is due to the gas flow friction and in *(1-α)* portion of the time, in which the liquid phase contacts the walls, the pressure gradient is due to liquid friction. Using Eq.(4), assuming u_l and u_g would be the same, the above equation for slug flow can be rewritten as

$$(\frac{\Delta P}{\Delta x})_{2\Phi} = \frac{32G}{D^2}(\frac{\alpha\mu_g + (1-\alpha)\mu_l}{\alpha\rho_g + (1-\alpha)\rho_l}) \tag{6}$$

Kawahara *et al.* (2002) compared six different relations for two-phase homogenous viscosity models to find the pressure gradient. Five models had more than 100% error; however, the homogenous model of Dukler *et al.* (1964) for viscosity that is the same as that presented here (Eq. 6), $(\mu=\alpha\mu_g+(1-\alpha)\mu_l)$, had the best agreement with the experimental data (within ±20%). However, in the procedure of finding Eq.(6) we did not use any homogenous flow assumption. The fully developed and parallel flow assumptions for each phase is not valid near the gas-liquid interface and because of this fact the experimental pressure drop data show the factor of 30.08 instead of 32.0 in Eq.(6), which is 6% lower than that of the conventional correlation (Kawahara *et al.*, 2002).

2.2 Flow Area Expansion Analysis, Single Phase

Fig. 2 shows a schematic of the flow through a typical flow area expansion. The target control volume stretches from the area change position to a downstream location at which it is assumed that the flow reaches a fully-developed state.
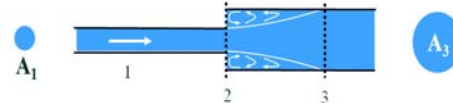

Fig. 2. Schematic of single phase flow through an expansion.

Applying the one-dimensional conservation of energy equation for the control volume shown in Fig. 2 leads to the following:

$$(p_1 + \frac{1}{2}\hat{\alpha}_1\rho_1 u_1^2) - (p_3 + \frac{1}{2}\hat{\alpha}_3\rho_3 u_3^2) = k_e\rho_{ave}\frac{u_1^2}{2} \tag{7}$$

So

$$k_e = \{(p_1 + \frac{1}{2}\hat{\alpha}_1\rho_1 u_1^2)$$
$$- (p_3 + \frac{1}{2}\hat{\alpha}_3\rho_3 u_3^2)\} / \{\rho_{ave}\frac{u_1^2}{2}\} \tag{8}$$

where k_e is the expansion loss coefficient and ρ_{ave} is the average density in the expansion area. $\hat{\alpha}_1$ and $\hat{\alpha}_3$ are kinetic energy correction factors, which can be defined as

$$\hat{\alpha} = \frac{\oint \rho u^3 dA}{\rho A u_{ave}^3} \tag{9}$$

where u_{ave} is the average velocity. When $u=u_{ave}$ that is uniform flow, $\hat{\alpha} = 1.0$. For laminar flow though a round pipe $\hat{\alpha} = 2.0$ and for turbulent flow $\hat{\alpha} = 1.05$. Now, applying the one-dimensional conservation of momentum equation

$$M_1 + M_3 = F_{p1} - F_{p3} \tag{10}$$

$$-k_{d1}\rho_1 A_1 u_1^2 + k_{d3}\rho_3 A_3 u_3^2 = P_1 A_3 - P_3 A_3 \tag{11}$$

Where k_{d1} and k_{d2} are momentum correction factors, which are defined as

$$k_d = \frac{\oint \rho u^2 dA}{\rho A u_{ave}^2} \tag{12}$$

When $u=u_{ave}$ that is uniform flow, $k_d = 1.0$. For laminar flow though a round pipe $k_d = 1.33$ and for turbulent flow (*1/7* law profile), $k_d = 1.02$.

By dividing both sides of Eq.(11) by A$_3$,

$$P_1 - P_3 = -k_{d1}\rho_1\sigma u_1^2 + k_{d3}\rho_3\sigma^2 u_3^2$$
$$= u_1^2(\sigma^2\rho_3 k_{d3} - \sigma\rho_1 k_{d1}) \tag{13}$$

where the area ratio is defined as

$$\sigma = \frac{A_1}{A_3} \tag{14}$$

Therefore Eq.(8) can be written as

$$k_e = \frac{u_1^2}{2}(\sigma^2\rho_3 k_{d3} - \sigma\rho_1 k_{d1} + \hat{\alpha}_1\rho_1 - \hat{\alpha}_3\rho_3\sigma^2)$$
$$/(\frac{1}{2}\rho_{ave}u_1^2) \tag{15}$$

For an incompressible flow this equation leads to

$$k_e = \sigma^2(2k_{d3} - \hat{\alpha}_3) + \hat{\alpha}_1 - 2k_{d1} \tag{16}$$

and if a flat velocity profile is assumed (which is common practice for the definition of loss coefficient), this equation leads to the Borda-Carnot relation

$$k_e = (1 - \sigma)^2 \tag{17}$$

In this study, to have consistency with the collected data of Toufik (2008), the same simple relation was used to compare our modeling results to the experimental data. Therefore, both modeling and experimental loss coefficients can be found by combining Equations (8) and (17) as follows:

$$k_e = \frac{\Delta P}{\frac{1}{2}\rho u_1^2} - \sigma^2 + 1 \tag{18}$$

Where ΔP is either the modeling or experimental pressure difference across the expansion area. In this relation several simplifying assumptions were applied. All correction factors of momentum and kinetic energy were assumed to be unity. Moreover, this relation inherently assumes that the flow is incompressible, which is valid for the liquid phase. However, for the gas phase this assumption may not be valid under some conditions. When frictional loss is included, as it must be for a very long and narrow pipe, the incompressible flow analysis previously considered applies until the pressure drop does not exceed 10% of the initial pressure (ASHRAE, 2001). Since compressibility makes the analysis very complicated, Toufik (2008) assumed that the gas phase behaves as incompressible and Kawahara *et al.* (2002) used the average gas density between inlet and the outlet conditions of the pipe to calculate the loss coefficient. However, in the next section we will show that the incompressible assumption is not valid for two-phase slug flows through a sudden area change, since the density ratio of phases is on the order of O(1000), providing a sharper gradient of pressure

along the channel.

2.3 Flow Area Contraction Analysis, Single Phase

It is common practice that the converging section of the flow (until the *vena contracta*) in which deceleration takes place from the *vena contracta* to the fully-developed flow region can be modeled as flow through a sudden expansion (Kays, 1950). According to this assumption, expansion after the vena contracta to the downstream region can be modeled similarly to that in the flow expansion that was mentioned in the previous section. For incompressible flows it can be written as:

$$k_c = \frac{1 - (\alpha_1\sigma^2 - 2k_{d1} + 1 - \sigma^2)C_c^2 - 2C_c}{C_c^2} \tag{19}$$
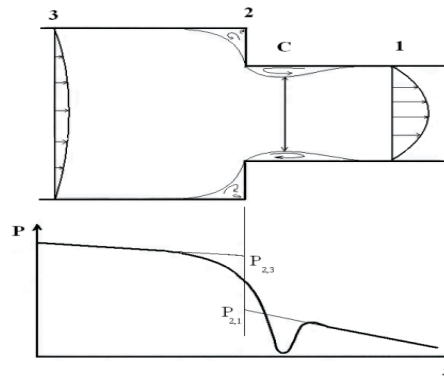
Fig. 3. Schematic of single phase flow in Contraction.

where $C_c = A_c/A_1$, is the Vena-contraction coefficient. Geiger (1964) suggested an experimental correlation for C_C

$$C_c = 1 - \frac{1 - \sigma}{2.08(1 - \sigma) + 0.5371} \tag{20}$$

In this study to have consistency with the collected data of Toufik (2008), the same simple relation was used to compare our modeling results to the experimental data. Therefore, both modeling and experimental loss coefficients have been calculated based on the $C_c = 1$ assumption as

$$k_c = \frac{\Delta P}{\frac{1}{2}\rho u_1^2} + \sigma^2 - 1 \tag{21}$$

2.4 Two-Phase Pressure Change across Area Change (Conventional Models)

It is common practice that using the same analysis for single-phase flows, the pressure drop in sudden expansions and contractions in two-phase flows without phase change and for flat velocity profiles, can be expressed as follows (see Abdelall *et al.*, 2005, Kawahara *et al.*, 2002, and Toufik, 2008):

$$\Delta P_e = P_{2,1} - P_{2,3} = G_1^2 (\frac{\sigma^2}{\rho'_3} - \frac{\sigma}{\rho'_1})$$

(22)

where G_1 is the mixture mass flux in the smallest channel and subscripts refer to Stations 1 and 3 in Fig. 2. The quantity ρ' is the momentum density which was defined by Lahey and Moody (1993) according to the following equation:

$$\rho' = [\frac{1-x^2}{\rho_l(1-\alpha)} + \frac{x^2}{\alpha\rho_g}]^{-1}$$

(23)

where x is the vapor mass quality and α is the void fraction of the flow. Toufik *et al.* (2008) assumed that if both phases are incompressible, x and α both would remain constant during the flow area expansion and contraction. So Eq.(22) can be simplified to

$$\Delta P_e = G_1^2 (\frac{\sigma^2 - 1}{\rho'})$$

(24)

In the next section we will show that in microchannels assuming constant α during the expansion or contraction may not be valid since each phase accelerates or decelerates at a different rate because of the different densities, wall shear forces and viscosity. In order to use the above equation, a closer equation needs to correlate vapor mass quality to the void fraction. The quality-void relation for one-dimensional flows is related to the slip ratio "S" according to the following:

$$S = \frac{x}{1-x} \frac{1-\alpha}{\alpha} \frac{\rho_l}{\rho_g}$$

(25)

For homogenous flows $S=1$. Two-phase flows across sudden contractions are considerably more complicated than those across sudden enlargements. In the flow area contraction in two-phase flows, it is still unclear whether the characteristics of the vena-contracta in two phase flow are the same as those of single phase flows. However, for two-phase flows, in analogy with single-phase flows using the vena contracta concept, Collier (1972) and Hewitt *et al.* (1993) suggested the following:

$$\Delta P_c = G_1^2 [\frac{\rho_h}{2} (\frac{1}{C_c^2 \rho''^2_{2,1}} - \frac{\sigma^2}{\rho''^2_3}) + (\frac{1}{\rho'_1} - \frac{C_c}{\rho'_{2,1}})]$$

(26)

where G_1 is the mixture mass flux and C_c is the coefficient of contraction which is a function of the area ratio. Chisholm (1983) recommended

$$C_c = \frac{1}{0.639\sqrt{1-\sigma} + 1}$$

(27)

where ρ_h is the average homogenous flow density between Points 2 and C (the minimum area) which can be found from the average slip ratio between these points

$$\rho_h = \rho_l(1-\alpha) + \rho_g\alpha$$

(28)

and

$$\rho'' = [\frac{(1-x)^3}{\rho_l^2(1-\alpha)^2} + \frac{x^3}{\rho_g^2\alpha^2}]^{-\frac{1}{2}}$$

(29)

Also the momentum density ρ' is defined in Eq.(23) and void fraction α is defined as

$$\alpha = \frac{x\rho_l}{S\rho_g(1-x) + \rho_l x}$$

(30)

in which, *x,* is the vapor mass quality.

With the same analogy for the pressure drop in the pipe, effective mixing caused by sudden contraction may justify the assumption of homogenous flow, and leads to

$$\Delta P_c = \Delta P_l \phi_l$$

(31)

$$\Delta P_c = \frac{G_1^2}{2\rho_l}[(\frac{1}{C_c^2} - 1)^2 + (1 - \sigma^2)]$$

(32)

$$\phi_l = 1 + x(\rho_l - \rho_g)/\rho_l$$

(33)

However, Schmidt and Friedel (1997) have shown that the *vena contracta* phenomenon may not occur in two-phase flow at all. In the next sections we will introduce an analytical model for slip ratio value in *vena contracta* location. We will then introduce a new model for pressure drop in contraction for two-phase slug flow in microchannels.

2.5 New Analytical Model for Void Fraction in Contraction

As we have shown for pressure drop in the straight microchannel pipe flow, if the flow behaves like the slug flow, the nature of flow is similar to a pulsing flow and the frequency of the pressure pulses in the vicinity of the contraction depends on the length and velocity of liquid and gas slugs. In all cases, not only does void fraction not remain constant but the two-phase flow regime may also change from that of a big pipe to that of a small pipe. Fig. 4 shows a schematic of the flow in a microchannel with a sudden contraction. We are assuming that the liquid slugs are incompressible while gas slugs are compressible.

Even though the constant static pressure far upstream of the contraction is not a perfect assumption for this pulsating type flow, because of the friction, damping, and simplicity we have set the far upstream pressure constant while the downstream pressure was allowed to oscillate. Since we are looking for the pressure difference between the up- and downstream locations, we expect that this assumption would not have a major effect on the final results since with a simple shifting we can set either the downstream or upstream pressure as the reference pressure

Even though obtained results show that all movements and oscillations have been affected by gas and liquid slug's length in the bigger pipe, published experimental work does not reveal much information on these lengths or correlate them to the other properties. For a fixed gas slug length, L_G,

liquid slug length, L_l, is just a function of quality (or void fraction). However, from experimental photographs in the literature, gas slug length varies from 1 to 15 times the pipe diameter (see Fig. 1) and for this case we have assumed the initial length of the gas slug to be seven times that of the bigger pipe diameter, D_3, and for different qualities, the corresponding liquid slug lengths could be calculated. At this point we recommend for that subsequent experimental studies provide detailed information on the time-averaged values of slug lengths under different conditions.

The proposed model assumes that the liquid slug hits the facing wall of the contraction at $t=0$ and after this point, the velocity of the center of mass of the liquid slug and those of the front and tail of this slug as well as the pressure and velocity of the gas slug following the liquid slug would be monitored until the latter passes the contraction and reaches a steady state condition.
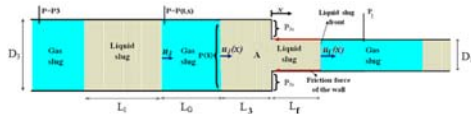

Fig. 4. Schematic of two-phase slug flow in a microchannel facing a contraction.

A brief algorithm of the present model is shown in Fig. 5. The gas slug pressure behind the target liquid slug is characterized by an equation of state. If the ideal gas assumption is assumed to apply on the gas slug, the pressure can be expressed as

$$P(x) = \rho(x)RT \tag{34}$$

The liquid slug's center of mass location is determined by

$$X_c = \frac{\rho_l}{2m_l}(A_1 L_f^2 - A_3 L_3^2) \tag{35}$$

where ρ_l and m_l are liquid slug density and mass, respectively. L_f and L_3 were defined in the schematic in Fig. 4. The center of mass velocity, u_c, can be obtained by differentiating Eq. (35) with respect to time. Applying the continuity equation to the liquid slug, the front liquid slug velocity in the smaller pipe, u_f, can be correlated to the center of mass velocity by this nonlinear relationship

$$u_f = (\frac{m_l}{\rho_l A_1})\frac{u_c}{(L_f + L_3)} \tag{36}$$

When liquid slug is going through the contraction, the pressure in the vicinity of the front walls reaches values very close to the stagnation pressure. The actual integration of the numerical results (CFD modeling which is not presented in this paper) over this surface reveals that the average pressure on this wall is almost 94 percents of the stagnation pressure and slightly changes by changing the area ratio. However, for simplicity we have assumed that this pressure is the same as the stagnation pressure.

On the other hand nonlinear shear forces act on the liquid slug. For laminar flows, the friction factor, f, is a sole function of the Reynolds number. For turbulent flow, which is the case here since the diameter is very small, the fully-rough wall assumption is appropriate. Thus, the Colebrook's natural roughness function that is independent of the Reynolds number, have been used to describe the friction as

$$\frac{1}{\sqrt{f}} = 1.14 + 2\log(D/\varepsilon) \tag{37}$$

Conventional values of turbulent and laminar Reynolds numbers in two-phase slug flows may be questionable since there is no obvious length scale to define the Reynolds number. One can define it based on the diameter of the pipe while because the small length of the slugs (the same order of the diameter) one may prefer to define it based on the average length of the slugs. Moreover, it seems that if we fix our frame of reference on the moving slugs, because of the short length of the slugs, most or all of the slug length would be in the developing region. This indicates that the length of the slug plays an important role in slug flows. While this seems to be the case, no one seems to have reported on the time-averaged values of the slug length.

Because of this fact, even for laminar flow, since it is expected that for the most part the slug is located in the developing region in which the velocity gradient and consequently the overall friction factor are greater than what is expected from the parabolic velocity profile for laminar flows, Eq.(37) may present a closer approximation of the real friction factor for slug flows.

As can be seen in the schematic figure and algorithm, since the net forces and moving mechanism are different before and after passing of the liquid slug tail from the contraction area, calculations should be performed separately for these regions (see the algorithm)

As long as the liquid slug tail travels in the bigger pipe, the front velocity and the center of mass velocity will correlate well with Eq. (36) and the net force acting on the liquid slug can be calculated as follows:

$$\Sigma F = (P - P_{ave})A_3 - \pi(D_1 L_f F_{f1} + D_3 L_3 F_{f3}) \tag{38}$$

where F_f is the wall shear stress, P is the variable gas slug pressure and P_{ave} is the average pressure acting on the front face of the contraction. They can be calculated from the following equations:

$$F_f = \frac{1}{8}\rho_l f u_f |u_f| \tag{39}$$

$$P_{ave} = P_{3s}(1-\sigma) - P_i\sigma \tag{40}$$

In each time step, the liquid slug center of mass velocity can be calculated based on the momentum
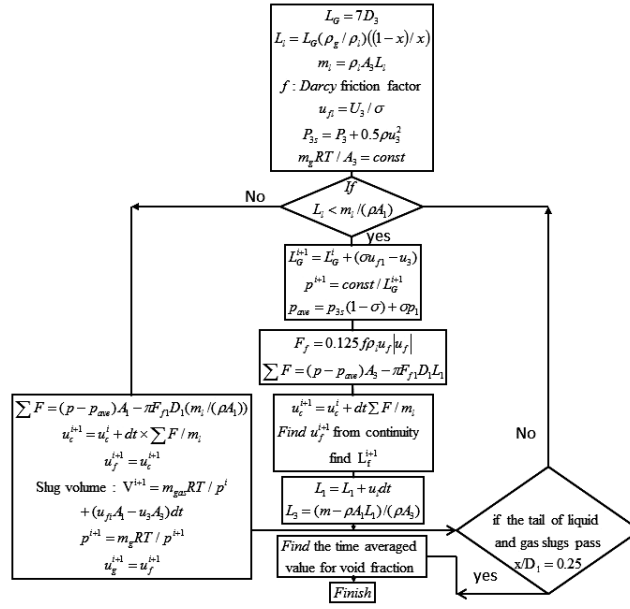
Fig. 5. Summary of algorithm used for modeling the average void fraction in the vicinity of the flow area contraction.

change and the net forces acting on the slug

$$u_c^{i+1} = u_c^i + \frac{\sum F}{m_l} dt \qquad (41)$$

where $i, i+1$, represent the current and next time steps, respectively. Then the front velocity, u_f, would be obtained from Eq. 36 and the tail velocity can be easily found by $u_3(x)=\sigma u_f$. With knowing the tail velocity, $u_3(x)$, the gas slug pressure can be calculated by finding the volumetric compression of the gas slug. Therefore, applying the equation of state for an ideal gas, the following correlation can be obtained

$$P^{i+1} = (\frac{m_g RT}{A_3})/(L_3^i + dt(\sigma u_f^i - u_3)) \qquad (42)$$

where m_g is the gas slug mass (using the initially $7D_3$ assumption for the gas slug length mentioned earlier). Since walls periodically wet and dry with the liquid and gas slugs, it is expected that for such a small diameter, the temperature of the gas slug would remain constant, hence, in developing Eq.(42), we have assumed that this process is almost isothermal. This seems to be valid for small compression ratios, but it may not be valid for cases that include phase change between vapor and liquid slugs where the mass of the gas slug would not be conserved anymore. These processes continue until the liquid slug tail passes the bigger diameter pipe and enters the smaller pipe. Then the net force acting on the liquid slug can be calculated from

$$\Sigma F = (P - P_j)A_1 - \pi D_1 L_{l1} F_f \qquad (43)$$

where L_{l1} is the liquid slug length in the smaller pipe. Practically P_j is the gas slug pressure subsequent to the liquid slug; however, for simplicity since the gas slug length is very long in

comparison with the diameter of the smaller pipe, it can be assumed that P_j is equal to the downstream pressure P_1. So as we mentioned, calculation starts when the liquid slug hits the facing walls of the contraction at $t=0$ (s). At this stage $L_f=0$ (Figure 4) but the front velocity is $u_f=u_3/\sigma$ and the tail velocity at this infinite small time is equal to u_3 (boundary conditions).
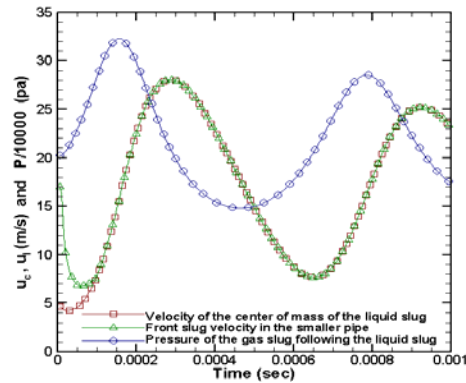
Fig. 6. Gas slug pressure, liquid center of mass velocity and liquid front velocity.

Because the gas viscosity is much smaller than that of a liquid, the gas slug can travel through in the contraction rapidly while the liquid slug (having the higher momentum (Order (1000))) hits the front walls of the contraction and produces pressure waves that are directly transferred from the incompressible liquid slug to the gas slug and causes a phenomenon similar to that of a water hammer but with smaller magnitudes. This is because gas slugs are much more elastic than liquid slugs and this fact reduces the strength of the pressure waves. Water slugs pass through the

contraction with more restriction due to the larger friction and the smaller average pressure difference on both sides of the liquid slug (Eq. (43)). This causes a small chocking and reduction in the liquid slug velocity. On the other hand, the slugs that follow come with higher velocities and compress the gas slug behind the liquid slug passing through the contraction. The gas slug pressure, P, increases until the liquid slug completely gets inside the smaller pipe. Then the gas slug that follows, which has already been compressed, shoots the liquid slug in the smaller pipe. Because of this fact, the shooting speed of the liquid slug exceeds the steady state velocity of the downstream flow, which leads to a decrease in the pressure of the gas slug that follows, while the wall shear force is also affecting the slug motion. This spring-damper type (here spring behavior of gas slug is not linear) of oscillation may continue until the wall shear force damps this oscillation and the liquid slug velocity reaches the steady state condition of the downstream flow.

This phenomenon can be seen in more detail in Fig. 6. In this figure the liquid slug's center of mass velocity, u_c, slightly decreases at the initial stages due to the chocking (adverse front wall forces and excess shear forces) that was mentioned earlier. This reduction would be sharper for the smaller area ratios, σ. The liquid front velocity in the smaller pipe initially starts from the steady state value in the small pipe and decreases sharply due to the reduction of u_c as well as the change in the center of mass position that is dynamically moving. After passing the contraction, both the slug's center of mass velocity and the front velocity become equal after the oscillation to be damped by the wall friction. Since the pressure-volume relation and damping forces are not linear, none of these oscillations are sinusoidal in nature, thus, all the main frequencies can be extracted with a Fast Fourier Transform algorithm.

To find the gas void fraction at the *vena contracta*, knowing the location of the *vena contracta* is important. Although extensive experimental studies have been reported on air-water two-phase flows in mini and microchannels, there seems to still exist considerable discrepancies, largely due to the difficulties in experimental setup and measurements (Kandlikar, 2002 and He and Kasagi, 2008). To understand the detailed physics of slug flow in microchannels, advanced numerical simulations were performed to help develop a more precise analytical model. Numerical studies on single-phase air-water flows, showed that for turbulent water flow the position of the minimum cross sectional area (due to the *vena contracta*) occurs at $0.25D_1$ downstream of the sudden contraction (this number for laminar flow is $0.15D_1$) and the minimum cross sectional diameters are $0.85D_1$ and $0.92D_1$ for turbulent and laminar flow, respectively. The conventional definition of the slip ratio is the ratio of the time-averaged value of the gas phase velocity to the liquid phase velocity. For a small pressure drop it is common practice that the compressibility effects

be neglected. However, this assumption is not valid in the vicinity of the contraction where the pressure gradient is significant. Especially in two-phase flows the density ratio between phases is typically in the order of 1000 and all changes take place in considerably shorter distances, thus, the variation of the gas density could not be neglected. With this analytical model the length of liquid and gas slugs can be determined at any time. Therefore, if compressibility effects of the gas slug were taken into account, the time-averaged void fraction in the *vena contracta* may be expressed by the time averaging of the volume of the gas slug.

Time-averaged void fraction of the gas slug in the vicinity of the *vena contracta* location ($x=0.25D_1$) can be calculated from

$$\bar{\alpha} = \frac{\int_0^{t_2} V_G(t)dt}{\int_0^{t_2} V_f dt + \int_0^{t_2} V_G(t)dt} \tag{44}$$

where V_G and V_f are the gas and liquid slug volumes, respectively. Time starts when the gas-liquid interface reaches the *vena contracta* location, while t_2 corresponds to the time that the tail of the two liquid and gas slugs that follow pass the *vena contracta* location.

2.6 New Pressure Drop Model for Slug Flow through a Contraction in Microchannels

Pressure drop across sudden contraction for two-phase flow assuming overall long and short slug flow regimes can be determined by the same concept that was used for the singular pipe. Pressure drop through the contraction for a single-phase flow can be found using Eq.(32). So for the flat velocity profile which is a reasonable assumption for slug flow in an α portion of time, the pressure drop is due to the gas phase motion, and in (1- α) portion of time, the pressure drop is due to the liquid phase motion, so the time-averaged pressure drop can be written as

$$\Delta P_{c-2\Phi} = \frac{u_1^2}{2}(1 + (1 - \frac{1}{C_c})^2 - \sigma^2)$$
$$\{\rho_g \alpha + \rho_l (1 - \alpha)\} \tag{45}$$

where C_c was defined in Eq. (27) and u_1 is velocity of slugs in the smaller pipe. This was defined in Eq. (4) and α is the void fraction in the vicinity of the *vena contracta*, which can be found from the new analytical model of averaged void fractions presented in the previous section. It is well known that void fraction values around the *vena contracta* controls the pressure drop. Different empirical void fraction models can be found in the literature; however each model is valid for a specific regime or experimental condition. Moreover, these models are tuned for straight pipe flows. As mentioned earlier, for the sudden area change it is common to use one of those correlations to find an expression that makes a better

fit for the experimental data (see Chalfi and Ghiaasiaan, 2008, Abdelall *et al.*, 2005, Kawahara *et al.*, 2002, Hewitt *et al.*, 1993, and Collier, 1972). So, a good amount of the previous work is practically based on curve fitting of existing void fraction or slip ratio correlations for the straight pipe to the experimental data associated with the flow in contractions. However, the one-dimensional model discussed in the previous section showed that the gas phase accelerates quicker than the liquid phase in a sudden contraction due to the lower density and wall shear forces. These analyses led to introducing a new model for the void fraction in the vicinity of the contraction. In the following, results of the new models for void fraction and pressure drop (Eq. (45)) will be compared to the conventional models and experimental data.

Abdelall *et al.*'s (2005) experimental data were used for evaluating the model in this paper. In their experiment, Abdelall *et al.* (2005) determined the pressure drop using linear interpolation of the pressure data up and downstream of the contraction (Fig. 3). Two-phase regime maps in microchannels are slightly different than those of macrochannels mainly due to the larger surface tension effects and the reduced gravitational forces. Kawahara *et al.* (2002) studied the flow regime map for a 100 *μm* diameter pipe and compared it to other available maps for microchannels. The closest map to Abdelall *et al.*'s (2005) test rig is the test case of Tripllet *et al.* (1999) whose data were obtained for a 1.1 *mm* diameter tube (close to the average diameter of Abdelall *et al.*'s test rig). Therefore, it is expected that Fig. 7 would show the overall flow regime map of this case study. It can be seen that all of the data in the bigger pipe (upstream of the contraction) are in the slug or ring-slug flow modes, which makes them more appropriate for our model. The downstream regime, on the other hand, is in multiple zones, which means that all bubbly, ring-slug, slug annular, churn, annular and slug flows can be observed and our model for the slug flow may not be appropriate. However, since there is a transitional process for regime change and we are just looking to examine the *vena contracta* location, which is located a short distance downstream of the contraction, it can be expected that the flow regime would not change from the initial slug regime state to a completely multiple zone regime in this short distance. Also, even if it changes, since we are time averaging void fractions through the contraction process, the side effects of this issue would be damped with this integration.

Fig. 8, shows the relation between the void fraction *α* and homogenous void fraction *β* (slip ratio *S=1*) using different models for α and/or slip ratio, *S*. Armand (1946) proposed α=0.833 β for the conventional tube.

Based on the experimental data of a *100 μm* diameter tube Kawahara *et al.* (2002) introduced the following equation:
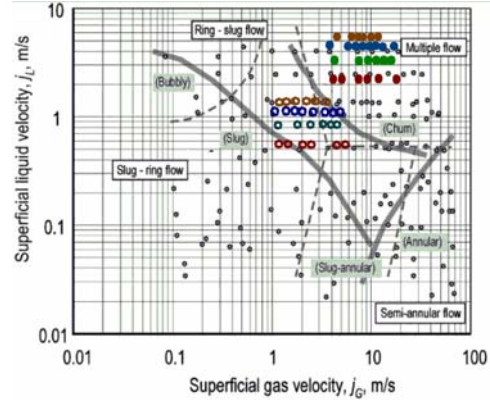
Fig. 7. Two-phase flow regime map for a 1.1 mm diameter tube, Triplett *et al.* (1999) Bold big circles are Abdelall *et al.*'s (2005) data which were used for the analytical model (Hollow big bold circles are for the larger diameter pipe and solid big bold circles are for the smaller diameter pipe).

$$\alpha = \frac{0.03\beta^{0.5}}{1 - 0.97\beta^{0.5}} \qquad (46)$$

For the annular flow when the minimum entropy generation rule is applied, Zivi (1964) introduced the following expression for the slip ratio

$$S = c\left(\frac{\rho_l}{\rho_g}\right)^{1/3} \qquad (47)$$

where *c=0.7* in the modified model. If curve fitting were to apply on the data points to minimize the error in the pressure drop using the presented model in Eq. (45), the following correlation can be proposed for the average void fraction in the vicinity of the contraction area for β>0.4

$$\alpha = \frac{0.5 - 0.47\beta^{0.5}}{1 - 0.97\beta^{0.5}} \qquad (48)$$

All of the above correlations (except the curve fit) were tuned for the straight pipe flow. However, the new analytical model for the void fraction (Equations 34 to 45) was obtained based on the slug and semi-slug flow assumptions in which the void fraction dynamically changes in the transitional area due to the difference in acceleration or deceleration of each phase

Calculated averaged void fractions with the proposed dynamic model are shown in Fig. 8. As can be seen, for this area ratio and flow conditions, the data correlate well in the high volume-fraction region and correlate well with the Armand correlation for the smaller volume–fraction region. Moreover, against the other models, the dynamic model's data are not on a line or a special curve and the data depend on the flow conditions as well as the geometrical constrains. It is interesting that the

results of the new analytical model show outstanding agreement with the experimental curve fit, so it seems that it can describe the physics of this phenomenon quite well.
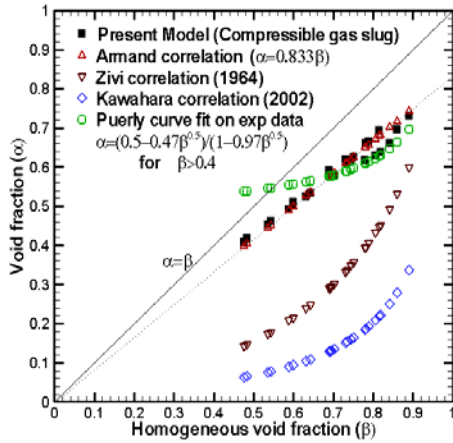
Fig. 8. Relationship between homogeneous void fraction and void fraction for different models in the vicinity of the flow area contraction.
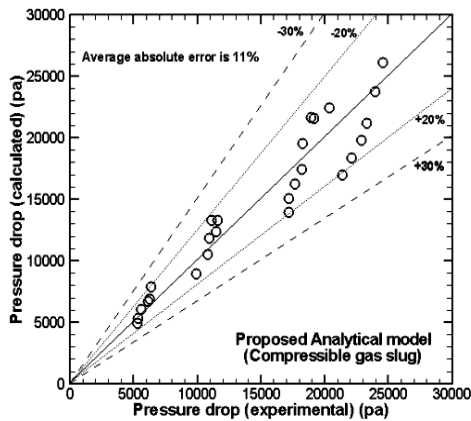
Fig. 9 (a). Comparison of six void fraction models (New analytical model).
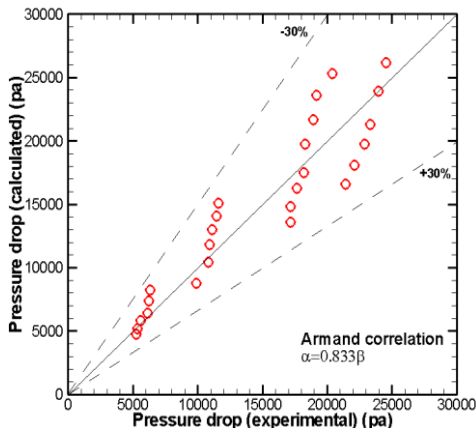
Fig. 9 (b). Comparison of six void fraction models (Armand's correlation).
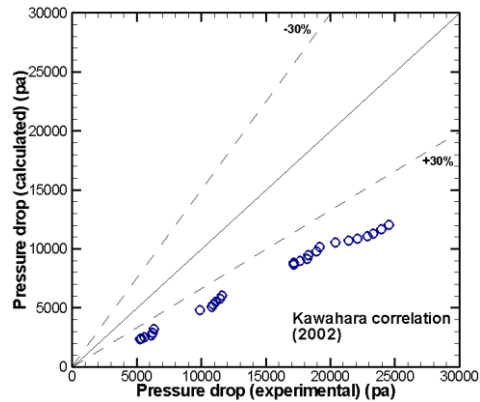
Fig. 9 (c). Comparison of six void fraction models (Kawahara *et al.*'s correlation).
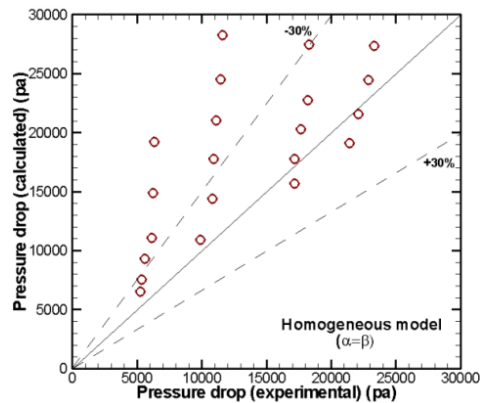
Fig. 9 (d). Comparison of six void fraction models (Homogeneous model).
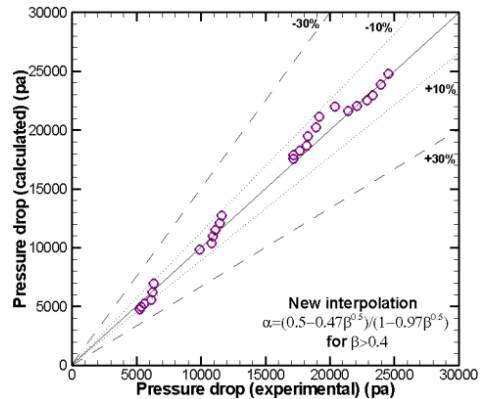
Fig. 9 (e). Comparison of six void fraction models (Pure curve fit of experimental data).

Fig. 9 illustrates a comparison of different models with the experimental data for the pressure drop across the sudden contraction in microchannels. Before taking a look at the details, it can be seen that all of six figures show the robustness of Eq. (45) for slug flows. If we compare the maximum error in these figures with the latest conventional models (Eq. (26)), that were applied by Chalfi and Ghiaasiaan (2008) and Abdelall *et al.* (2005) who reported 500% error for the homogenous model and 100% error for the slip flow models, the robustness

of the proposed model for pressure drop should be clear. These figures show that the presented model (Eq.(45)) is robust enough that the maximum error would not exceed than 310% (for the homogenous model) regardless of what model is used to calculate the void fraction, α, at the *vena contracta* location.
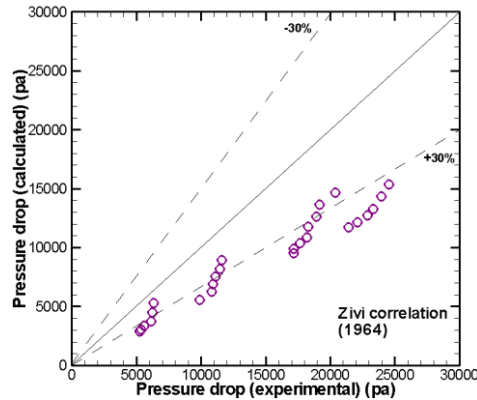
Fig.9 (f). Comparison of six void fraction models (Zivi's correlation).
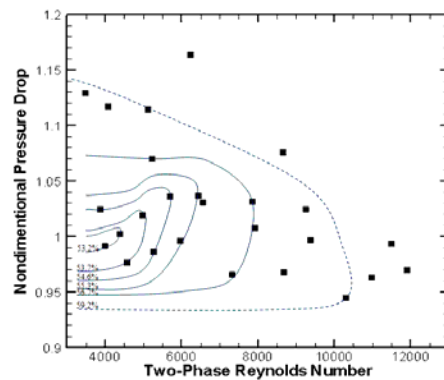
Fig. 10. Nondimentional pressure drop versus two-phase Reynolds number for the experimental data of Abdelall *et al*. (2005). The constant void fraction lines are also shown here.

In Fig. 9(d), it can be seen that the homogenous model has the worst accuracy. The error in the Kawahara *et al*.'s correlation in Fig. (9)b is also significant. Chalfi and Ghiaasiaan (2008) and Abdelall *et al*. (2005) reported 100% error for the pressure drop using Zivi's model for α using the conventional model for the pressure drop, however, in Fig. 9.f it can be seen that Eq. (45) could reduce the maximum error to 50%.

Armand's correlation in Fig. 9(b) which was used by Chalfi and Ghiaasiaan (2008) and Abdelall *et al*. (2005) and was their most accurate model which showed 30% error, with the presented model shows 20% error.

With a curve fit and tuning based on the experimental data defined by Eq. (48), the error in

the presented model can be reduced to 8% which is shown in Fig. 9€.

As was mentioned earlier, all of the above models are either based on the empirical model or the homogenous model and more importantly they were tuned for the straight pipe flow. But the new purely analytical model for the void fraction could have a good agreement with experimental data (see Fig. 9(a). After curve fitting the data (Fig. 9.e) this analytical model has the second most accurate prediction and reduced error to 20%. More importantly, since this is an analytical model, all changes in the flow properties and different geometrical constrains can also be monitored and studied. Furthermore, it can provide better understanding of the physics taking place in slug flows facing the contraction that were harder to study before using the more conventional models.

Pressure drop in nondimensional form versus the two-phase flow Reynolds number can be seen in Fig. 10. Nondimensionalization is obtained based on the new correlation introduced in Eq.(45) in which Eq.(48) is used to define the gas void fraction, α, in the vicinity of the contraction along with the total mass flux, *G*. So, the nondimensional pressure drop is defined as

$$P^* = \frac{\Delta P_{\exp}(\alpha \rho_g + (1-\alpha)\rho_l)}{\frac{1}{2}G^2(1-\sigma^2)}$$

(49)

While the two-phase Reynolds number is defined as

$$\mathrm{Re}_{2\phi} = (\alpha(\frac{\rho_w}{\mu_w}) + (1-\alpha)(\frac{\rho_g}{\mu_g}))u_1 D_1$$

(50)

It can be seen that all nondimensional values of the pressure drop are in the range between 0.945 and 1.16 (close to unity). Also the data are showing a weak function of the two-phase Reynolds number which indicates that this nondimensional parameter for the pressure drop is the main nondimensional parameter. To have more precise prediction of the pressure drop, some curves can be introduced to distinguish the data based on their void fraction values. It can be seen that for any given two-phase Reynolds number there are two possible regions for the nondimensional pressure drop. This may come from the fact that for any given two-phase Reynolds number in reality there are two different gas-liquid slug lengths. The smaller length of liquid slug corresponds to the larger pressure drop and vice versa. So it seems that with additional experimental data about the slug length, the pressure drop in slug flows in microchannels can be more precisely predicted to even have better accuracy than the current accuracy (8% error). So to achieve this goal many experiments should be conducted on the slug lengths.

3. CONCLUSIONS

In this paper a new analytical model for void fraction calculation was developed. The model revealed some important phenomena that are occurring in two-phase slug flows through a sudden area contraction. Against the previous models which used slip ratio correlations of straight pipes for the flow in the contraction, the new model directly tackled this problem and provided accurate predictions of the void fraction. Moreover, based on the new model, we were able to find the value of the real void fraction in the vicinity of the *vena contracta*, which helped to develop another correlation for the pressure drop in two-phase slug flows through the area contraction. Results showed excellent progress in pressure drop prediction. This new model could reduce the minimum (60%) and maximum (500%) errors of the more conventional models to a minimum of 8% and a maximum of 310%.

REFERENCES

Abdelall, F. F., G. Hahn, S. M. Ghiaasiaan, S. I. Abdel-Khalik, S. M. Jeter, M. Yoda and D. L. Sadowski (2005). Pressure drop caused by abrupt flow area changes in small channels, *Experimental Thermal and Fluid Science* 29, 425-434.

Armand, A. A. (1946). The resistance during the movement of a two-phase system in horizontal pipes, *Izv. Vses. Teploteck. Inst.* 1, 16-23 (AERE-Lib/Trans 828).

ASHRAE Handbook: Fundamentals. (2001). *The American Society of Heating, Refrigerating and Air-Conditioning Engineers, Inc.*, Atlanta, GA.

Chalfi, T. Y. and Ghiaasiaan, S. M. (2008). Pressure drop caused by flow area changes in capillaries under low flow conditions, *Int. J. Multiphase Flow*. 34, 2-12.

Chaoqun, Y., Z. Yuchao, Y. Chunbo, D.Minhui, D. Zhengya and C. Guangwen, (2013). Characteristics of slug flow with inertial effects in a rectangular microchannel, *Chemical Engineering Science* 95, 246–256.

Chisholm, D. (1983). Two-phase flow in pipelines and heat exchangers, *Pitman Press*, Bath, England.

Collier, J. G. (1972). Convective boiling and condensation, *Published McGraw-Hill Book Co*, UK.

Damianides, C. A. and J. W. Westwater (1988), Two-phase flow patterns in a compact heat exchanger and small tubes. *Proceedings of Second UK National Conference on Heat Transfer*, Glasgow, September 14-16, Mechanical Engineering Publications, London, 1257-1268.

De, S., C. K. Sandra, G. Heynderickx, J. Marin and B. Guy (2008). CFD modeling of all gas-liquid and vapor-liquid flow regimes predicted by the Baker chart. *Chemical Engineering Journal*. 138, 349-357.

Dukler, A. E., I. M. Wicks and R. G. Cleveland (1946). Frictional pressure drop in two-phase flow: a comparison of existing correlations for pressure loss and holdup. *AIChE J.* 10(1), 38-43.

Fukagata, K., N. Kasagi and P. Ua-arayaporn (2007). Numerical simulation of gas-liquid two phase flow and convective heat transfer in a micro tube. *Int. J. Heat Fluid Flow*. 28, 72-82.

Fukano, T. and A. Kariyasaki (1993). Characteristics of gas-liquid two-phase flow in a capillary. *Nuclear Engineering Design*. 141, 59-68.

Geiger, G. E. (1964). Sudden contraction losses in single and two-phase flow. Ph.D. thesis, University of Pittsburgh, Pittsburgh, PA.

Ghiaasiaan, S. M. and S. I. Abdel-Khalik (2000). Two-phase flow in microchannels. *Advances in Heat Transfer*. 34, 145-254.

He, Q. and N. Kasagi (2008). Phase-field simulation of small capillary-number two-phase flow in a microtube. *Fluid Dynamics Research*, Vol. 40, No. 7-8, July-August 497-509.

Hewitt, G. F., G. L. Shires and T. R. Bott (1993). *Process heat transfer*. CRC Press, Ann Arbor, Michigan, ISBN 9780849399183.

Kandlikar, S. G., (2002). Fundamental issues related to flow boiling in mini channels and microchannels. *Experimental Thermal and Fluid Science*. 26, 389-407.

Kawahara, A., P. M. Y. Chung and M. Kawaji (2002). Investigation of two-phase flow pattern, void fraction and pressure drop in a microchannel. *Int. J. Multiphase Flow*. 28, 1411-1435.

Kawahara, A., M. Sadatomi and A. Shimokawa (2012). Lengths of bubble and slug and pressure drop in gas-liquid slug flow in microchannels. *Multiphase Science and Technology*. 24 (3), 239–256.

Kays, W. M. (1950). Loss coefficient for abrupt changes in flow cross-section with low Reynolds number flow in single and multiple tube system. *Trans. ASME*. 72, 1067-1074.

Lahey Jr., T. R. and F. J. Moody (1993). The thermalhydraulic of boiling water nuclear reactors. *2nd Ed., American Nuclear Society*, La Grange Park, Illinois.

Schmidt, J. and L. Friedel (1997). Two-phase pressure drop across sudden contraction in duct areas. *Int. J. Multiphase Flow*. 23, 283-299.

Serizawa, A., Z. Feng and Z. Kawara (2002). Two-phase flow in microchannels. *Experimental Thermal and Fluid Science*. 26, 703-714.

Triplett, K. A., S. M. Ghiaasiaan, S. I. Abdel-Khalik and D. L. Sadowski (1999). Gas-liquid two phase flow in microchannels-Part I: Two-phase flow pattern. *Int. J. Multiphase Flow*. 25, 377-394.

Yao, C., Z. Dong, Y. Zhao and G. Chen (2014). The effect of system pressure on gas-liquid slug flow in a microchannel. *AIChE Journal*. 60 (3), 1132-1142.

Zhao, T. S. and Q. C. Bi (2001). Co-current air water two-phase flow pattern in vertical triangular microchannels. *Int. J. Multiphase Flow*. 21, 765-782.

Zivi, S. M. (1964). Estimation of steady-state steam void-fraction by means of the principle of minimum entropy production. *J. Heat Transfer*. 68, 247-252